Nanopix v1: a compact miniaturized coded aperture gamma imager

Guillaume Amoyal, Vincent Schoepff, Frédérick Carrel, Lionel Tondut, Christopher Helbert, Michael Fiederle, Alexander Fauler, Johann Plagnard, Roger Abou-Khalil, Zakkarya Mekhalfa, et al.

Nanopix-v1: a compact miniaturized coded-aperture gamma imager.

G. Amoyal[(a)], V. Schoepff[(a)], F. Carrel[(a)], L. Tondut[(b)], C. Helbert[(c)], M. Fiederle[(d)], A. Fauler[(d)], J. Plagnard[(e)], R. Abou-Khalil[(f)], Z. Mekhalfa[(f)], M. Imbault[(a)], Q. Adeline[(a)].

[(a)] *Université Paris-Saclay, CEA, List, F-91120 Palaiseau, France.*

[(b)] *Orano Business Unit Recycling, DT/E/MN/EXP, F-50440 La Hague, France.*

[(c)] *Orano DS – DTI/ICM, F-50440 La Hague, France.*

[(d)] *Freiburger Materialforschungszentrum, Albert-Ludwigs-Universität Freiburg, D-79104 Freiburg, Germany.*

[(e)] *Université Paris-Saclay, CEA, List, Laboratoire National Henri Becquerel (LNE-LNHB), F-91120 Palaiseau, France.*

[(f)] *Orano Group, 125 Avenue de Paris, Châtillon 92320 France.*

ABSTRACT

This article explores the complex challenges associated with detecting and identifying radioactive hotspots in the nuclear industry using gamma cameras. Gamma cameras facilitate the localization of radioactive hotspots by overlaying a visualization of radioactivity onto a visible image. In the nuclear industry, gamma rays are observed in an energy range spanning from 59.5 keV (Am-241) to 1.3 MeV (Co-60).

The motivation for this exploration stems from a specific challenge: characterizing hot-cells inaccessible to human operators. At the ORANO La Hague radioactive waste reprocessing plant, access to these restricted regions is possible through apertures with diameters ranging from 8 to 10 cm. In collaboration, the Nanopix-v1, characterized by its compact form as a coded mask gamma imaging system, with dimensions of 8×5.1×4.3 cm³ and a mass of 268 g, was developed through the synergistic efforts of CEA List and X-ray Imaging Europe (XIE) in partnership with ORANO.

This article conducts a detailed examination of the laboratory and in situ performance of the Nanopix-v1, carried out within the challenging operational environment of the La Hague radioactive waste reprocessing plant. The focal point of the article is a comprehensive exploration of the technological components supporting the Nanopix-v1, along with an explanation of the coded mask imaging localization methodologies that underpinned the rigorous evaluation process. The performance of the gamma camera is evaluated through a series of carefully conducted trials, aimed at evaluating the angular resolution and minimum measurement time, including laboratory conditions, experimentation within a metrological Cs-137 irradiator, and practical implementation at the ORANO La Hague site.

I. INTRODUCTION

The detection and precise identification of radioactive hotspots present a formidable challenge across various domains within the nuclear industry, encompassing radiation protection measurements within nuclear power plants, decommissioning operations, responses to post-accidental events like the Fukushima incident, and applications vital for Homeland Security. Addressing this challenge necessitates the utilization of transportable and readily deployable systems. One efficacious solution lies in the deployment of gamma cameras, capable of superimposing gamma ray images onto visible images to pinpoint radioactive hotspots within their field of view.

Within the context of applications at the La Hague radioactive waste reprocessing site, the prominent French entity ORANO articulated the imperative to access zones with heightened radioactivity, ascertain the presence of radioactive hotspots, and respond promptly. Access to these zones is exclusively attainable via chute holes characterized by diameters ranging from 8 to 10 cm, thereby requiring a compact gamma camera with at least two of its geometric dimensions measuring below 8 cm.

In recent years, several research teams have dedicated their efforts to the development of Compton or coded aperture gamma-ray imagers tailored explicitly for use in the nuclear industry. CEA List, for instance, embarked on the development of a coded aperture gamma camera named GAMPIX in the late 2000s [1–3]. Subsequently, MIRION Technologies undertook the industrialization of this CEA List prototype, and it is now available in the commercial market under the name iPIX [4]. The iPIX camera measures 9.0×9.0×18.8 cm³ in terms of its dimensions. Notably, other gamma imaging systems designed for nuclear industry applications have emerged, including the ASTROCAM 7000HS by Mitsubishi Heavy Industries, (44.5×34.0×23.5 cm³), NuVISION [5] by NUVIA (12.0×24.0×18.0 cm³), POLARIS H [6] by H3D (24.0×8.6×18.0 cm³), Spid-X by 3D Plus Detection Systems (18.0×11.0×32.3 cm³), and Temporal Delta by DAMAVAN (21.0×29.0×16.0 cm³), to name a few.

It is noteworthy that the geometric dimensions of the existing industrial gamma imaging systems mentioned above render them unsuitable for access to the areas of interest within the La Hague facility. In close collaboration with ORANO, CEA List has ingeniously developed a compact coded mask gamma imaging system, christened Nanopix-v1, sharing technological components

with the GAMPIX gamma camera. Eventually, the Nanopix-v1 system boasts dimensions of 7.9×5.1×4.3 cm³, a mass of 268 g, and a field of view of 44°. Nanopix-v1 is able to locate gamma-rays emitters whose energy range from 59.5 keV (Am-241) up to 1.3 MeV (Co-60) with an angular resolution around 5°.

This article primarily centers on the comprehensive developments surrounding Nanopix-v1, encompassing an evaluation of its performance within laboratory settings and the La Hague site. In paragraph II , we will delve into the foundational building blocks of Nanopix-v1, elaborate on the coded mask imaging localization techniques employed alongside Nanopix-v1, and outline the methodologies employed for performance assessment. Subsequently, paragraph III will focus on the experimental evaluation of the Nanopix-v1 gamma camera's performance, commencing with laboratory conditions and progressing to the evaluation of its response within the LNHB (Henri Becquerel National Laboratory) metrologically qualified Cs-137 irradiator, extending to assessments conducted at the ORANO La Hague site.

II. Material and Methods

A. Nanopix-v1 gamma coded-aperture gamma imager

1) Building blocks of Nanopix-v1

The foundational element of Nanopix-v1 is the detector board, responsible for providing measurement data. Gamma rays, measured in the nuclear industry, span an energy range from 59.5 keV, attributed to Am-241, to 1.3 MeV, associated with Co-60. To tackle this challenge, the selected detector is a modified USB Lite readout interface [7], incorporating a Timepix ASIC [8]. Timepix, a pixelated counting chip, operates in frame-based mode, comprising 256×256 pixels with a 55 µm pitch, allowing for the measurement of the position and energy deposited by ionizing particles. The sensitive component of the detector block is a 1-mm thick high-resistivity p-type cadmium telluride semiconductor, bump-bonded to Timepix. This particular sensor was chosen for its intrinsic performances, aligning most effectively with the challenges associated with detecting gamma rays in the nuclear industry [9]. The integrated source of detector bias within the USB Lite can provide a 5 to 100 V, which is not enough to bias the 1-mm thick CdTe semiconductor, that requires a bias of -300 V. Therefore a USB driven external power supply is mounted on the USB Lite. A cooling bridge is also mounted on the assembly in order to keep the detector block at room temperature. The detector block, composed of the USB Lite module and the Timepix ASIC hybridized with a 1-mm thick CdTe semiconductor, the cooling bridge and the external power supply is shown in Figure 1. The USB Lite module embedded in Nanopix-v1 is not energy calibrated, however, it has been estimated that its low energy threshold is around 10 keV.

Table I: Characteristics of USB Lite readout interface [7].

Serial redout speed	4 Mbit/s (4 fps)
Integrated source of detector bias	5 – 100 V.
Dimensions	15×60 mm²
Data transfer	USB

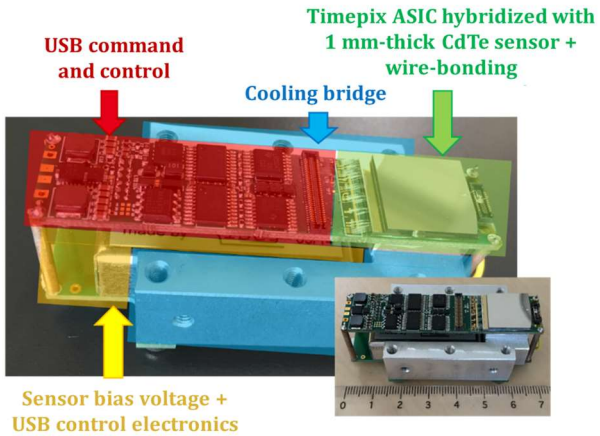

Figure 1: The detector block of Nanopix-v1, composed of a USB Lite module, an external power supply and a cooling bridge.

The two other building blocks associated with the pixelated detector (i.e., Timepix) to build a gamma imager are the coded aperture and the visible camera. The coded aperture consists of a rank 7 MURA coded aperture [10], with a thickness of 4 mm, made of tungsten alloy. The choice of the coded aperture is based on previous studies around the GAMPIX gamma camera [2] and results from a trade-off between the minimum time of measurement and angular resolution over the energy range of measured gamma-rays in the framework of nuclear industrial applications. The dimensions of the coded aperture pattern are such that the fully-coded field of view covers the whole sensor [11], and the central part of the coded-aperture basic pattern has the dimensions of the sensor [12]. This results in a coded-aperture pattern with dimensions of 2.8×2.8 cm², and composed of 13×13 individual aperture cell of

0.2154 cm pitch. The distance between the sensor and the coded-aperture is 1.4 cm, providing a fully-coded field of view of 44°. Eventually, the manufactured coded-aperture with dimensions of 3.4×3.4×0.4 cm^3 and a total mass of 48 g.

Regarding the visible camera, a research effort on compact visible optics enabled to significantly reduce its dimensions. By positioning it as close as possible to the detector interface card (a few millimeters), unused internal spaces can be removed. Thus, the size of the gamma camera is mainly determined by the detection block shown in Figure 1. Figure 2 shows the Nanopix-v1 gamma camera, (a) a footprint drawing is presented, and (b) and (c) show two pictures of Nanopix-v1 from two different perspectives. The final dimensions of Nanopix-v1, with all building blocks integrated, are 7.9×4.3×5.1 cm^3, for a total mass of 268 g.

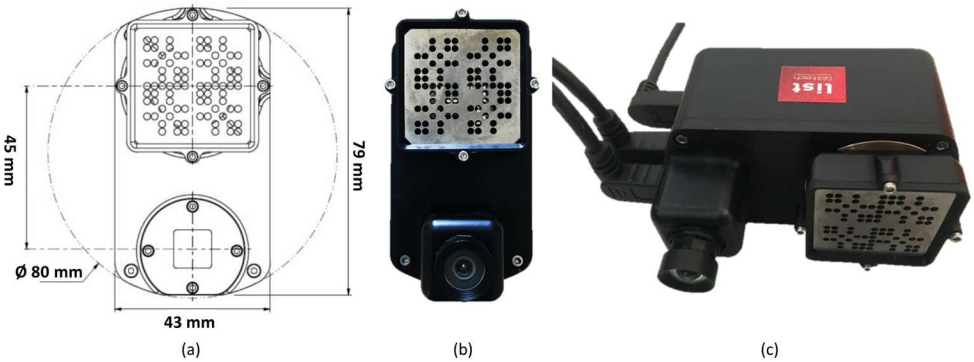

Figure 2: (a) Footprint drawing of Nanopix-v1 gamma camera, (b) and (c) photographs of Nanopix-v1 from two different perspectives.

Table II: Main characteristics of Nanopix-v1.

Sensor	CdTe – 14.08×14.08×1 mm^3
Pixelisation	256×256 pixels – 55 µm pitch
Coded aperture	MURA rank 7 in tungsten, thickness: 4 mm
Field of view	44°
Communication protocol	USB
Dimensions	7.9×4.3×5.1 cm^3
Weight	268 g
Low energy treshold	~ 10 keV

2) Raw frame analysis

When a gamma ray interacts with the CdTe semiconductor, Timepix provides information about the position of the interaction and the energy deposited within the sensor, in the form of a frame composed of 256×256 pixels. In Timepix, the energy of the interaction is measured using a Time-over-Threshold (ToT) method [13]. The ToT value for each interaction is measured by a clock, whose frequency is set at 40 MHz. This results in a ToT value of 25 ns, which represents the amount of time that the signal from the interaction is above a given threshold. The ToT value is proportional to the energy deposited in the detector by the interaction, and can be used to determine the energy spectrum of the incident radiation.

The Nanopix-v1 yields measured data in the form of a 256×256 ToT value matrix. When a particle interacts with the CdTe semiconductor, it may illuminate several adjacent pixels, resulting in a cluster of pixels. To determine the energy deposited by the particle, it is necessary to identify each pixel cluster, which is achieved through the utilization of the DBSCAN algorithm [14]. Figure 3 demonstrates the application of the DBSCAN algorithm to identify pixel clusters within a measured frame. The frames displayed in Figure 3 (76×66 pixels) are a subset of an entire measured frames (256×256 pixels).

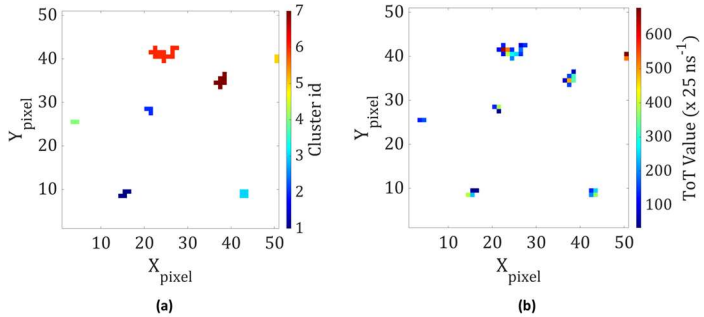

Figure 3: Representation of cluster identification using DBSCAN algorithm, on the left-hand side, a measured frame with ToT values assigned to each pixels; on the right-hand side, pixels that belong to the same cluster are identified by assigning the same color.

After identifying the different clusters of pixels in a given frame, the ToT spectrum is reconstructed by summing the ToT values of each cluster. Examples of measured ToT spectra using Am-241, Cs-137, and Co-60 sources are shown respectively in Figure 4 (a), (b) and (c). In the Am-241 ToT spectrum, two peaks are clearly distinguishable: the peak with the highest ToT values (in red) corresponds to the full absorption peak at 59.5 keV, while the peak with the lowest ToT values (in blue) corresponds to a mixture of X-ray fluoresence lines of cadmium and telluride (K shell lines), along with their associated escape peaks. The Cs-137 ToT spectrum highlights the full absorption peak at 661.7 keV in red. However, in the Co-60 ToT spectrum, the full absorption peaks at 1.173 MeV and 1.332 MeV are not reconstructed, and only the Compton edges can be identified. For Co-60 gamma-rays, Compton scattering is the main interaction occurring within the semiconductor, and once scattered, photons may be absorbed. Since the positions of the Compton scattering and the absorption are different, the pixel clusters resulting from these interactions cannot be geometrically joined and identified as a single interaction, resulting in the total absorption peak being unreconstructed.

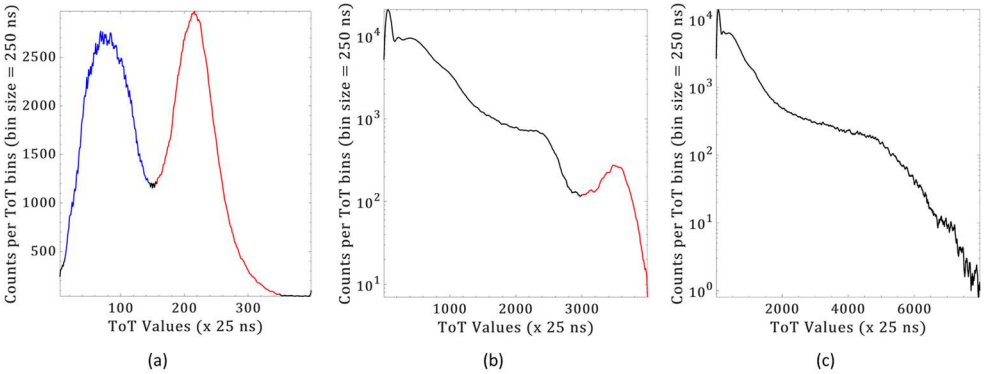

Figure 4: Examples of ToT spectra measured with Nanopix using Am-241 (a); Cs-137 (b); Co-60 (c) sources.

3) Coded-aperture imaging with Nanopix-v1

Gamma cameras using coded-aperture employ a spatial modulation imaging technique where a coded-aperture made up of a specific pattern of opaque and transparent elements is positioned between the sensitive detection area and the radioactive source. This results in the photons emitted by the source projecting a shadowgram of the coded-aperture pattern on the detection area. The Nanopix-v1 gamma camera uses a MURA coded-aperture and the decoding algorithm proposed in [10], based on a convolution product between the shadowgram and the matrix describing the coded-aperture pattern. This algorithm involves convolving the shadowgram with a decoding function represented by the coded-aperture pattern. To eliminate gamma background caused by radioactive sources outside the gamma camera's field of view and also compensate the coded-aperture transparency when the energies of gamma-rays increases, we employ the "mask/anti-mask" procedure (MAM), which involves taking a second measurement after rotating the mask by 90° [10]. Therefore, for a given measurement, two shadowgrams are measured: one for the “mask” measurement, and a second one for the “anti-mask” measurement. Then, the “anti-mask” shadowgram is subtracted to the “mask” shadowgram. In its current stage, the “mask/anti-mask” procedure is not automated, and the mask should be rotated or by means of an external system.

A ToT discrimination may also be applied on the interaction of interest used to build the shadowgram, enabling spectral imaging. This feature can be of interest if multiple radionuclides are simultaneously present in the scene to be imaged.

From this shadowgram and by using knowledge of the coded-aperture pattern, the radioactive source can be reconstructed in a decoded image [10,11]. The decoded image is obtained by performing a convolution operation between the shadowgram, which is a matrix of 256 × 256 cumulated ToT values per pixel, and the Point Spread Function (PSF), described by the mask pattern. The result of this convolution is a new matrix of 256 × 256 ToT values that represents the decoded image. The hotspot, which corresponds to the position with the highest intensity in the decoded image, represents the location of the radioactive source.

Once the decoded image is reconstructed, a threshold may be applied to highlight the hotspot with respect to the background. The common threshold value with Nanopix-v1 is 50 % of the maximum value in the decoded image. This threshold value is chosen by default in our application for the reasons mentionned hereafter. Firstly, this serves to “eliminate” statistical noise in the reconstructed image. Secondly, it corresponds to the value of the Rayleigh criterion, where two peaks are considered separable. Using a threshold value of 50 % thus indirectly applies this criterion to the decoded image. However, the threshold value may be adjusted, notably, if several sources or extended sources are present in the reconstructed area.

Examples of a shadowgram and the associated normalised decoded image, with and without threshold, of a radioactive source located in the center of the Nanopix-v1 field-of-view are shown in Figure 5.

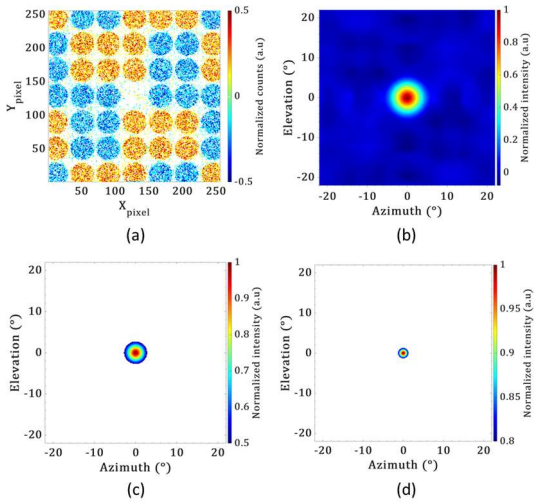

Figure 5: Examples of a shadowgram from a MAM procedure (a); (b) the associated decoded image without threshold; (c) the associated decoded image with a 50 % threshold; (d) the associated decoded image with an 80 % threshold. The radioactive source is located in the center of the field-of-view of the Nanopix-v1 gamma imager.

B. Angular resolution

In coded aperture gamma imaging, the angular resolution, expressed in degrees, defines the capability of a system to separate two elements in the decoded image. From a given geometry, composed of a planar detector and a planar MURA coded aperture, the theoretical angular resolution can be calculated from equation (II-1) [12]. In equation (II-1), θ_{geom} is the theoretical angular resolution, b is the dimension of an individual coded aperture cell, and z the aperture-to-detector distance. For Nanopix-v1, the dimensions of an individual aperture cell b is 0.2154 cm, and the aperture-to-detector distance z is 1.4 cm, providing a theoretical angular resolution of 4.41°. It has to be mentionned that this value only takes into account geometrical properties of the system, and does not take into account the aliasing of the coded-aperture and its transparency, that respectively depend on the source location and energy of the gamma-rays.

$$\theta_{geom} = \frac{b}{2*z} \text{ (rad)} \quad \text{(II-1)}$$

In this study, the angular resolution is evaluated experimentally. It is calculated from the horizontal hot spot profile (HHSP), and the vertical hot spot profile (VHSP) by means of a gaussian fitting on the profiles. Both profiles are extracted from the maximum of the decoded image. The angular resolution corresponds to the full width at half maximum (FWHM) of the fitted gaussian. To assess the uncertainty associated with the calculated FWHM, and so the uncertainty associated with the angular resolution, we perform bootstrap sampling [15]. The number of fit trials per boostrap sample to estimate the uncertainty of the gaussian fit is set arbitrarily to 500. The values in the decoded image are initially expressed in pixels and to convert these values in degrees, we use equation (II-2), in which A is the value in degree, B is a value in pixel, FoV corresponds to the fully coded field of view (i.e., 44°), N is the number of horizontal or vertical pixels (i.e., 256).

$$A = \frac{B \times FoV}{N} \text{ (°)} \quad \text{(II-2)}$$

C. Minimum measurement time

Minimum measurement time is defined as the minimum time required to locate a radioactive hotspot within the decoded image. It has to be mentionned, that for this study, the minimum measurement time is evaluated when the radioactive source is located in the center of the field of view.

This approach involves comparing the decoded image for a given measurement time (t_m) to a decoded image obtained for a measurement time where the hot point is correctly localized. If the two images correspond, then the time t_m is considered sufficient to locate the hot point. To evaluate the accuracy of hot point localization at time t_m, the operation is repeated N times using random frames, allowing the percentage of cases where the hot point is correctly reconstructed for the given $t_m$to be evaluated.

First, a measurement is carried out with a sufficient number of frames using the MAM procedure. For this study, the minimum measurement time is evaluated using laboratory radioactive sources, described in paragraph III.A, for which a set of 7200 frames of 1 s in “mask”, and 7200 frames of 1 s in “anti-mask” are measured, for a total of 14400 frames. This decoded image corresponds to the “reference” decoded image (RDI). The next step consists in comparing decoded image obtained for a given time of

measurement (DIGTM) to RDI. The comparison is carried out by means of two criteria. The initial metric we consider is the 2-D correlation coefficient R between DIGTM and RDI, which is defined by the Pearson's correlation described by equation (II-3). In this equation, X_{ij} represents the intensity of the (i,j)th pixel in image X, Y_{ij} represents the intensity of the (i,j)th pixel in image Y, and $\overline{X}$ and $\overline{Y}$ correspond to the average intensities of images X and Y, respectively. The 2-D correlation coefficient is a measure of the similarity between two images, which quantifies their correlation. It takes values between -1 and 1, where -1 indicates perfect inverse correlation, 0 indicates no correlation, and 1 indicates perfect direct correlation. The closer the value is to 1, the more similar the two images are, and vice versa for values close to 0. Negative values indicate inverse correlation between the images. For the study of the minimum measurement time, we chose a value of 0.5 to evaluate the similarity of the RDI and a DIGTM. At this stage of development, the value of the correlation criterion is chosen empirically. An additional study must be conducted to assess the impact of this value on the evaluation of the minimum measurement time.

$$R = \frac{\sum_i \sum_j \left(X_{ij} - \overline{X}\right)\left(Y_{ij} - \overline{Y}\right)}{\sqrt{\left(\sum_i \sum_j \left(X_{ij} - \overline{X}\right)^2\right)\left(\sum_i \sum_j \left(Y_{ij} - \overline{Y}\right)^2\right)}} \ (dimensionless) \qquad \text{(II-3)}$$

A second criterion is used in addition to the 2-D correlation coefficient, which is based on the number of hot spots reconstructed in the DIGTM. The DIGTM is considered correct only if a single hot spot is reconstructed, as there is by definition only one radioactive source positioned in the system's field of view. Examples of a RDI, and of a DIGTM fulfilling evaluation criterion, a DIGTM fulfilling the 2-D correlation criterion but not the criterion regarding the number of hostpots, and a DIGTM that does not meet both criteria are shown in Figure 6.

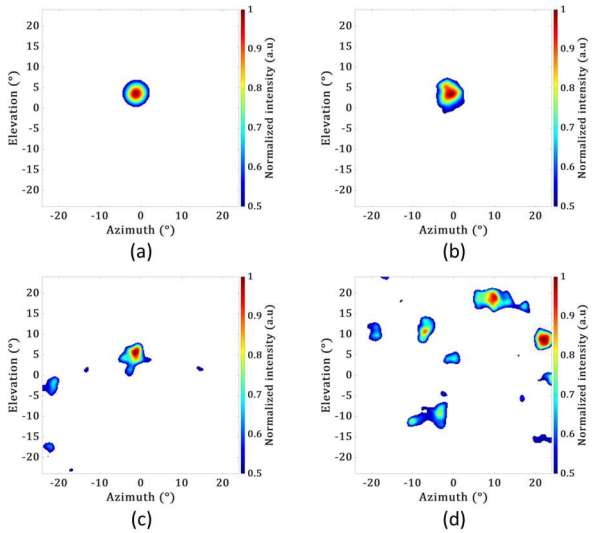

Figure 6: Examples of a reference decoded image with a threshold at 50 % (RDI) (a); a decoded image for a measurement time (DIGTM) fulfilling both criteria to validate the correct localization of the hot spot (b); a DIGTM fulfilling the 2-D correlation criterion but not the criterion regarding the number of reconstructed hot spots (c); and a DIGTM that does not meet the evaluation criteria (d).

In order to evaluate the reproductibility to correclty localizing a hot spot within a given time of measurement t_m, the operation is repeated 1000 times. The selection of frames for each repetitions is carried out by means of a random combination between the entire set of 7000 mask frames, and 7000 anti-mask frames. As an example, for a given measurement time t_m of 10 seconds, 5 mask frames and 5 anti-mask frames are randomly selected. Then, the percentage of DIGTM matching both evaluation criteria is calculated, providing a confidence percentage regarding the capability of the system to correctly reconstruct a hotspot in a given measurement time.

III. Experimental results

A. Laboratory measurement

1) Radionuclides

To experimentally characterize the Nanopix-v1 prototype in terms of minimum measurement time and angular resolution (as described in paragraphs II.B and II.C), the first step consisted in evaluating its performance on a large range of laboratory radioactive sources. The measurements were made using Am-241, Ba-133, Eu-152, Cs-137, and Co-60 radioactive sources, which are presented in Table IV along with their activities and equivalent dose rate H*(10) at one meter. These sources were selected because they cover a gamma energy range from 59.5 keV (Am-241) to 1.33 MeV (Co-60) and are commonly encountered in the nuclear industry. The Am-241, Ba-133, Cs-137 and Co-60 are encapsulated in stainless steel, whereas the Eu-152 source is

encapsulated in plastic. For this measurement campaign, the background noise corresponds to natural radioactivity and is less than 100 $nSv.h^{-1}$.

2) Angular resolutions

In this study, the horizontal and vertical angular resolutions of Nanopix-v1 were evaluated on the radionuclides described in Table III and by means of the method described in paragraph II.B. Table III present results regarding the horizontal and vertical angular resolutions obtained with Nanopix-v1. Results show that the horizontal and vertical angular resolutions are lower than 5.3°, and is slightly dependent on the energy of the incident gamma rays.

Table III: Horizontal and vertical angular resolutions evaluation for different radionuclides at a distance of one meter in the center of the field of view of Nanopix-v1.

	Angular resolution (°)	
Radionuclide	Horizontal	Vertical
Am-241	4.76 +/- 0.06	4.64 +/- 0.05
Eu-152	4.82 +/- 0.05	4.96 +/- 0.07
Ba-133	5.20 +/- 0.03	5.28 +/- 0.02
Cs-137	5.19 +/- 0.02	5.12 +/- 0.04
Co-60	4.77 +/- 0.08	4.85 +/- 0.06

3) Minimum measurement time

The method used in this study to evaluate the minimum measurement time of Nanopix-v1 relies on an evaluation of correctly reconstructed decoded image on a range of measurement time as described in paragraph II.C. The evaluation of the minimum measurement time of Nanopix-v1 was evaluated on the set of radionuclides described in Table IV.

The measurement protocol for each radionuclide is the following: the measurement is performed in "mask/anti-mask" (paragraph II.A.3)) with a frame duration of 1 second without ToT discrimination, the considered radionuclide is positionned in the center of the field of view of the coded-aperture at a distance of 1 m. Figure 7 shows the percentage of correctly reconstructed images versus measurement time for the aforementionned radionuclides.

Considering a 90 % confidence level on the reconstructed image, experimental results demonstrate that Am-241 positioned 1 m away from Nanopix-v1 (0.35 $\mu Sv.h^{-1}$) can be located in less than 2 s. In contrast, locating Eu-152 with an activity of 6.2 MBq at the same distance (1 m) from Nanopix-v1 (1.21 $\mu Sv.h^{-1}$) requires 12 s. Similarly, Ba-133, Cs-137, and Co-60, each with activities of 17.5 MBq (1.22 $\mu Sv.h^{-1}$), 34.3 MBq (3.30 $\mu Sv.h^{-1}$), and 10.4 MBq (4.94 $\mu Sv.h^{-1}$), respectively, can be located in 18 s, 54 s, and 130 s when positioned 1 m away from Nanopix-v1. From those values, the minimum measurement time at a 90 % confidence level per equivalent dose rate H*(10) unit for each radionuclide is calculated. This calculation provides the minimum measurement time to correctly localize a radionuclide in the center of the field of view with an equivalent dose rate at Nanopix-v1 of 1 $\mu Sv.h^{-1}$. Those values are summarized in Table IV.

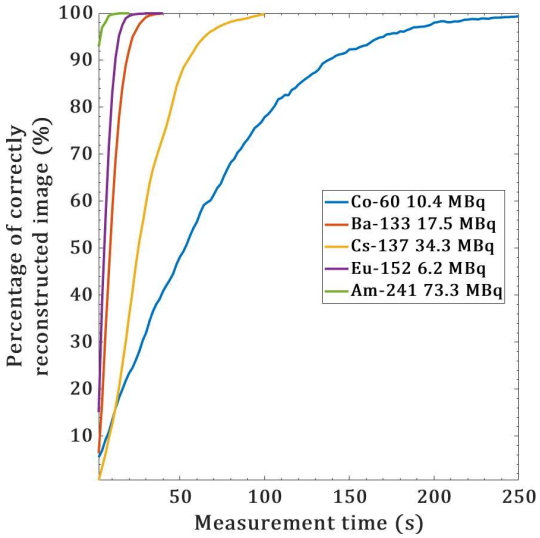

Figure 7: Percentage of correctly reconstructed images versus measurement time obtained with Nanopix-v1 for Co-60 (blue), Ba-133 (orange), Cs-137 (yellow), Eu-152 (purple) and Am-241 (green). Activities and equivalent dose rates H(10) at the Nanopix-v1 for each radionuclides are described in Table IV. For each measurement, the considered radionuclide is positioned at 1 m of Nanopix-v1 in the center of the field of view of the coded-aperture.*

Table IV: Minimum measurement time of Nanopix-v1 for different radionuclides with a confidence level at 90 %.

Radionuclide (activity in (MBq))	Equivalent dose rate H*(10)[1] at 1 m ($\mu Sv.h^{-1}$)	Minimum measurement time at a 90 % confidence level (s)	Minimum measurement time at a 90 % confidence level (s) per equivalent dose rate H*(10) unit ($s.(\mu Sv.h^{-1})^{-1}$)
Am-241 (73.3)	0.35	< 2	< 0.7
Eu-152 (6.2)	1.21	12	14
Ba-133 (17.5)	1.22	18	22
Cs-137 (34.3)	3.30	54	178
Co-60 (10.4)	4.94	130	642

[1]: Measured with a 6150 AD5/H radiameter from Saphymo©.

B. LNHB Cs-137 irradiator

A measurement campaign was carried out in a metrologically qualified Cs-137 irradiator to assess the response of Nanopix-v1 in terms of integrated dose. The Cs-137 irradiator is located at the LNHB, CEA List institute, Paris-Saclay site and is well known as one of the foremost national standards in the area of ionizing radiation. It is an essential component of the Laboratoire National de Métrologie et d'Essais (LNE), and it operates under the reference COFRAC accreditation. This accreditation delineates the range of validity of the primary references concerning dose rate.

The measurement campaign consisted in a set of 12 different measurements, whose objectives were to evaluate the behavior of Nanopix-v1 on a set of different dose rates. For each measurement, the integrated dose at Nanopix-v1 is known with a relative uncertainty of 5.7 % (k=2). The background noise is natural radioactivity (less than 100 $nSv.h^{-1}$). For a given measurement, the intensity (in ToT values as mentionned in paragraph II.A.3)) in the reconstructed hotspot is calculated by integrating the latter. To estimate the uncertainties on the numbers of hits in the hotspots, each measurement at a given dose rate is divided in sub-acquisitions whose measurement time is three times minimum measurement time of Nanopix-v1 to reconstruct an image at a 90 % confidence level for a given radionuclide (paragraph A.3)). To locate a Cs-137 with an equivalent dose rate H*(10) of 3.30 $\mu Sv.h^{-1}$ with a 90 % confidence level, Nanopix-v1 requires 54 s. Therefore, to locate a Cs-137 with an equivalent dose rate H*(10) of 33.4 $\mu Sv.h^{-1}$, we consider sub-acquisitions of $\frac{3.3}{33.4} \times 3 \times 54 = 16$ s. For each measurement, the measurement time is set in order to have at least 10 sub-acquisitions. For each sub-acquisition, the intensity (in ToT values) in the hotspot is calculated, providing a distribution. The agreement with a Normal distribution is verified using the Shapiro-Wilk test [16]. From this distribution, the mean value is calculated, and the associated uncertainty is estimated as twice the standard deviation (k=2). The intensities in the hotspots were evaluated over an integrated equivalent dose range extending from 83.2 nSv to 53.655 µSv, and are illustrated in Figure 8. The results show that the response of Nanopix-v1, with Cs-137, to the previously mentionned integrated equivalent dose is linear. Extrapolating the results from Figure 8, it is therefore possible to evaluate the equivalent integrated dose, and the equivalent dose rate of a Cs-137 hotspot at the Nanopix-v1 from the intensity of the considered hotspot.

It is planned to evaluate this response over a wider range of integrated dose in future work, and additionally over a wider set of radionuclides such as Am-241 and Co-60.

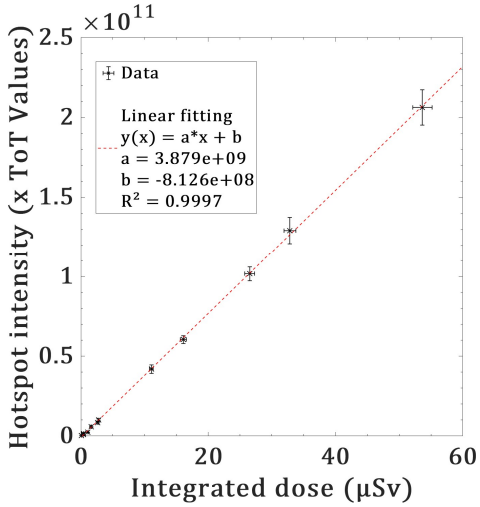

Figure 8: Hotspot intensity expressed in ToT Values versus integrated dose close to Nanopix-v1. The red dashed line represents the linear fit. Error bars are given 2 sigmas.

C. *In-situ measurement – ORANO La Hague.*

In this paragraph we present results obtained from in-situ measurements carried out with Nanopix-v1 at the nuclear materials recycling facility at ORANO La Hague, France. These measurements were carried out on a powder plutonium oxide (PuO_2) mixing hopper. This mixing hopper, located inside a shielded cell, roughly consists in a steel wheel with a 1 m diameter and a thickness of 50 cm with several blades aimed to mix the fresh PuO_2 powder. The powders enter through the upper part of the hopper, and are then mixed inside it. Once the powder is homogeneous, it is evacuated through a pipe located at the bottom of the hopper. The mass of the hopper is regularly checked to ensure that the powder is being properly evacuated. However, it appears that sometimes a portion of the powder remains blocked inside the hopper. To evacuate this powder, operators randomly strike the hopper with a hammer. The equivalent dose rate at the glove ports is around 240 $\mu Sv.h^{-1}$, limiting the intervention time of the operators to about ten minutes. The background noise in terms of equivalent dose rate in the shielded cell is around 150 $\mu Sv.h^{-1}$. The main purpose of these measurements with Nanopix-v1 was to locate the position within a hopper where PuO_2 powder had remained blocked, preventing its operation. It should be noted that this application case is a real case and was not specifically set up for this work. It illustrates a potential use case of interest involving the deployment of Nanopix-v1.

The first measurement involved localizing the blocked PuO_2 in the mixing hopper. The measurement protocol is as follows: Nanopix-v1 is positioned in front of the mixing hopper outside the shielded hot cell at a distance of one meter from the lead glass. The measurement consisted of 400 frames of 1 s using the "mask/anti-mask" procedure, i.e., 200 frames of 1 s in mask and 200 frames of 1 s in anti-mask. ToT spectra and decoded images presented in this section are obtained using the methods described respectively in paragraphs II.A.2) and II.A.3). Figure 9 shows the results of the first measurement: (a) the measured ToT spectrum on which two areas are highlighted, corresponding to ToT values used for ToT discrimination; (b) the decoded image; (c) and (d) show decoded images obtained using ToT discrimination, respectively, for the red and blue parts of the ToT spectrum. The crimson square displayed on the different decoded images correspond to the field of view of the gamma camera.

In the ToT spectrum (Figure 10 (a)), two areas of interest are highlighted:

- A red part with ToT values between 0 and 300, including two peaks. Since Nanopix-v1 is not energy calibrated, it is not possible to precisely convert those ToT values into energy. However, from the measured ToT spectrum of Am-241 shown in Figure 4 (a), we can deduce that both these peaks correspond to energies lower than roughly 70 keV. We made the assumption that these two peaks may originate partially from Am-241, Pu-241 daughter nuclide.
- A blue part corresponding to a Compton scattering zone, for which the time of measurement is insufficient to identify any total absorption peaks. We made the assumption that events depositing ToT values in this part correspond to fresh PuO_2 powder.

In the decoded image (Figure 10 (b)), a hotspot is located in the upper-right part of the mixing hopper. This hotspot corresponds to the blocked PuO_2 powder to be evacuated. Figure 9 (c) is the decoded image obtained using ToT discrimination. The events used are those whose ToT values are in the red part of the ToT spectrum. Two hotspots are located, one in the center of the mixing hopper, and a second one in the evacuation pipe. Those two hotspots correspond to "old" PuO_2 powder that has not been correctly evacuated from the mixing hopper. Figure 9 (d) shows the decoded image obtained by selecting events occurring in the blue part of the ToT spectrum. One hotspot is located, and confirms that the hotspot located without any ToT discrimination corresponds to the PuO_2 to be evacuated.

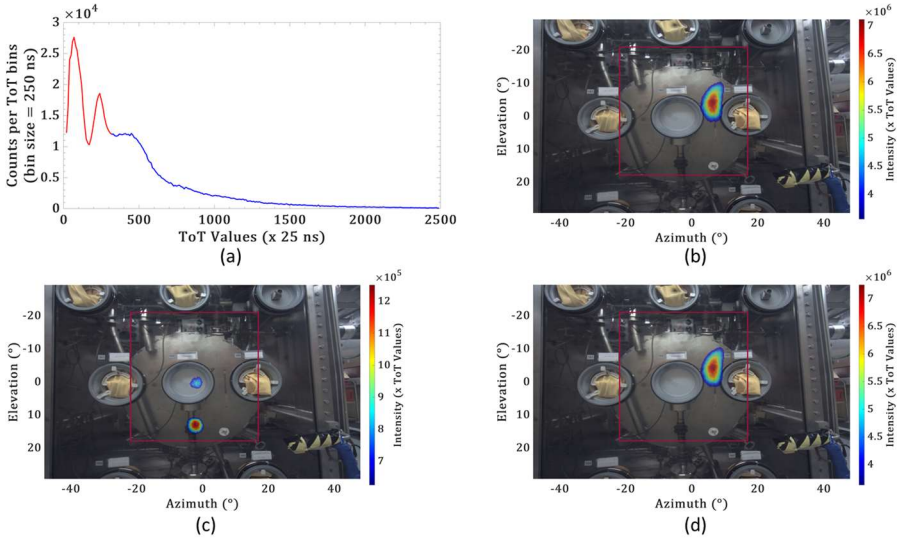

Figure 9: Localisation of blocked PuO_2 powder inside a mixing hopper at the ORANO, La Hague site using Nanopix-v1. Nanopix-v1 is positionned at a distance of 1 m, measurement consists in 200 frames in mask mode, and 200 frames in anti-mask mode. The duration of each frame is 1 s. In (a) the measured ToT spectrum; (b) the decoded image without ToT discriminitation; the decoded images obtained using ToT spectral discrimination, selecting events whose deposited ToT are in the red part (c) and blue part (d) of the ToT spectrum (a). On each decoded image, a threshold at 50 % of the maximum is applied.

Once the blocked PuO_2 powder was located using Nanopix-v1, the operators struck the hopper with a hammer at the appropriate spot to clear the blockage. A second measurement was then carried out to verify if the PuO_2 was successfully unblocked. The measurement protocol remained the same as the one described for the first measurement. Figure 10 shows the results of the second measurement: (a) the measured ToT spectrum on which two areas are highlighted, corresponding to ToT values used for ToT discrimination; (b) the decoded image; (c) and (d) show decoded images obtained using ToT discrimination, respectively, for the red and blue parts of the ToT spectrum. We can notice, by observing the field of view of the coded mask (represented by the crimson square on Figure 10 (b), (c) and (d)), that Nanopix-v1 was not positioned exactly at the same place for this second measurement. The interpretation of the ToT spectrum shown in Figure 10 (a) is the same as the one described for the first measurement, and will not be discussed for the second measurement. In the decoded image presented in Figure 10 (b), we can see that the hotspot is now in the bottom part of the hopper. We can deduce that the hammer strike on the hopper was efficient. On the decoded image presented in Figure 10 (c), resulting from a ToT discrimination, selecting only events depositing ToT values in the red part of the ToT spectrum, two hotspots are localised. The hotspot in the evacuation pipe is still at the same place, however the one in the center of the hopper is not here anymore. A second hotspot is visible in the lower part outside the hopper, and was not visible in Figure 9 (c). This is simply because as previously mentioned, Nanopix-v1 has been moved between the first measurement and the second measurement, and this part was not in the field of view of the coded-aperture in the first measurement. Figure 9 (d) shows the decoded image obtained by selecting events occurring in the blue part of the ToT spectrum. By comparing decoded image from Figure 9 (b) and Figure 9 (d), we can deduce that the hotspot shown in Figure 9 (b) is actually composed of two hotspots, one in the evacuation pipe, and the PuO_2 powder in the bottom part of the hopper.

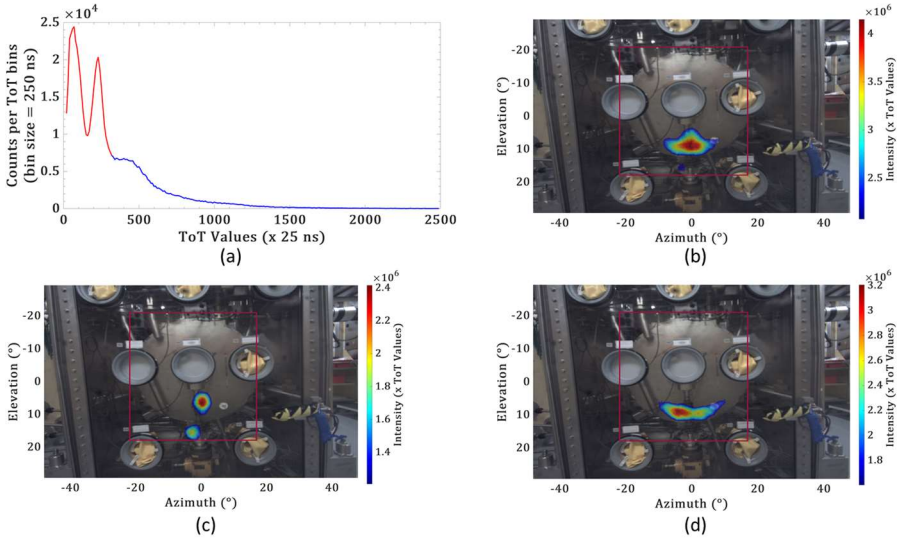

Figure 10: Localisation of PuO_2 powder inside a mixing hopper at the ORANO, La Hague site using Nanopix-v1 after striking the mixing hopper with a hammer to unstuck the powder. Nanopix-v1 is positionned at a distance of 1 m, measurement consists in 200 frames in mask mode, and 200 frames in anti-mask mode. The duration of each frame is 1 s. In (a) the measured ToT spectrum; (b) the decoded image without ToT discrimination; the decoded images obtained using ToT spectral discrimination, selecting events whose deposited ToT are in the red part (c) and blue part (d) of the ToT spectrum (a). On each decoded image, a threshold at 50 % of the maximum is applied.

IV. Conclusions and perspectives

In this work, we have developed a miniaturized coded-aperture gamma imager, Nanopix-v1, with dimensions of 7.9×4.3×5.1 cm^3, for a total mass of 268 g. Its performances in terms angular resolution and minimum measurement time have been evaluated on a set of commonly encountered radionuclides placed in the center of the field of view, covering a gamma energy range from 59.5 keV up to 1.33 MeV. We have also demonstrated the capability of the Nanopix-v1 to evaluate the equivalent integrated dose, and the equivalent dose rate of a Cs-137 hotspot at the Nanopix-v1 from the intensity of the considered hotspot. Eventually, in-situ measurements at the ORANO La Hague site have been performed with Nanopix-v1, showing the performances of Nanopix-v1 on a real use case.

A measurement campaing is planned with Nanopix-v1 on a dedicated installation to evaluate the performances in terms of angular resolution and minimum measurement time over a wider set of positions, particularly for off-axis sources. Future work will also be focused on energy calibrating the detector block, and evaluating the response in terms of Nanopix-v1 of dose rate on a larger set of radionuclides. A special effort will also be made in order to fully automatize the Nanopix-v1, integrating the rotation of the coded-aperture, and an embedded electronics for processing.

V. References

[1] F. Carrel, R.A. Khalil, S. Colas, D. De Toro, G. Ferrand, E. Gaillard-Lecanu, M. Gmar, D. Hameau, S. Jahan, F. Laine, A.S. Lalleman, F. Lemasle, C. Mahé, J.E. Maurer, N. Menaa, S. Normand, H. Onillon, N. Saurel, V. Schoepff, H. Toubon, GAMPIX: A new gamma imaging system for radiological safety and homeland security purposes, IEEE Nucl. Sci. Symp. Conf. Rec. (2012) 4739–4744. https://doi.org/10.1109/NSSMIC.2011.6154706.

[2] H. Lemaire, R.A. Khalil, K. Amgarou, J.C. Angélique, F. Bonnet, D. De Toro, F. Carrel, O. Giarmana, M. Gmar, N. Menaa, Y. Menesguen, S. Normand, A. Patoz, V. Schoepff, P. Talent, T. Timi, Implementation of an imaging spectrometer for localization and identification of radioactive sources, Nucl. Instrum. Methods Phys. Res. Sect. Accel. Spectrometers Detect. Assoc. Equip. 763 (2014) 97–103. https://doi.org/10.1016/j.nima.2014.05.118.

[3] G. Amoyal, V. Schoepff, F. Carrel, V. Lourenco, D. Lacour, T. Branger, Metrological characterization of the GAMPIX gamma camera, Nucl. Instrum. Methods Phys. Res. Sect. Accel. Spectrometers Detect. Assoc. Equip. 944 (2019) 162568. https://doi.org/10.1016/j.nima.2019.162568.

[4] K. Amgarou, A. Patoz, D. Rothan, N. Menaa, iPIX: A New Generation Gamma Imager for Rapid and Accurate Localization of Radioactive Hotspots, 2014.

[5] G. Montemont, P. Bohuslav, J. Dubosq, B. Feret, O. Monnet, O. Oehling, L. Skala, S. Stanchina, L. Verger, G. Werthmann, NuVISION: A Portable Multimode Gamma Camera based on HiSPECT Imaging Module, 2017 IEEE Nucl. Sci. Symp. Med. Imaging Conf. NSSMIC 2017 - Conf. Proc. (2018) 6–8. https://doi.org/10.1109/NSSMIC.2017.8532713.

[6] C.G. Wahl, W.R. Kaye, W. Wang, F. Zhang, J.M. Jaworski, A. King, Y.A. Boucher, Z. He, The Polaris-H imaging spectrometer, Nucl. Instrum. Methods Phys. Res. Sect. Accel. Spectrometers Detect. Assoc. Equip. (2014). https://doi.org/10.1016/j.nima.2014.12.110.

[7] Z. Vykydal, J. Jakubek, USB Lite — Miniaturized readout interface for Medipix2 detector, Nucl. Inst Methods Phys. Res. A 633 (2011) S48–S49. https://doi.org/10.1016/j.nima.2010.06.118.

[8] X. Llopart, R. Ballabriga, M. Campbell, L. Tlustos, W. Wong, Timepix, a 65k programmable pixel readout chip for arrival time, energy and/or photon counting measurements, Nucl. Instrum. Methods Phys. Res. Sect. Accel. Spectrometers Detect. Assoc. Equip. 581 (2007) 485–494. https://doi.org/10.1016/j.nima.2007.08.079.

[9] D. Maneuski, V. Astromskas, E. Fröjdh, E.N. Gimenez, J. Marchal, V. O'Shea, G. Stewart, N. Tartoni, Imaging and spectroscopic performance studies of pixellated CdTe Timepix detector, JINST 7 (2012). https://doi.org/10.1088/1748-0221/7/01/C01038.

[10] S.R. Gottesman, E.E. Fenimore, New family of binary arrays for coded aperture imaging, Appl. Opt. 28 (1989) 4344. https://doi.org/10.1364/ao.28.004344.

[11] E. Caroli, J. B. Stephen, G. Di Cocco, L. Natalucci, A. Spizzichino, Coded aperture imaging in X- and gamma-ray astronomy, 1987. https://doi.org/10.1007/BF00171998.

[12] S.R. Gottesman, A. Isser, G.W. Gigioli, N. Grumman, E. Systems, W.N. Rd, Adaptive coded apertures : bridging the gap between non-diffractive and diffractive imaging systems, 7818 (2010) 1–9. https://doi.org/10.1117/12.863032.

[13] J. Jakubek, Precise energy calibration of pixel detector working in time-over-threshold mode, Nucl. Instrum. Methods Phys. Res. Sect. Accel. Spectrometers Detect. Assoc. Equip. 633 (2011) S262–S266. https://doi.org/10.1016/j.nima.2010.06.183.

[14] M. Ester, H.-P. Kriegel, J. Sander, X. Xu, A Density-Based Algorithm for Discovering Clusters in Large Spatial Databases with Noise, in: Proc. Second Int. Conf. Knowl. Discov. Data Min., AAAI Press, 1996: pp. 226–231.

[15] P.D.W. Kirk, M.P.H. Stumpf, Gaussian process regression bootstrapping: exploring the effects of uncertainty in time course data., Bioinforma. Oxf. Engl. 25 (2009) 1300–1306. https://doi.org/10.1093/bioinformatics/btp139.

[16] S.S. Shapiro, M.B. Wilk, An Analysis of Variance Test for Normality (Complete Samples), Biometrika 52 (1965) 591–611. https://doi.org/10.2307/2333709.